RESEARCH ARTICLE

The **FASEB** Journal

Netrin-1 attenuates cerebral ischemia/reperfusion injury by limiting mitochondrial ROS and Ca^{2+} levels via activation of AKT phosphorylation and mitochondrial m-AAA protease AFG3L2

Xiaosheng Yang[1] | **Yang Liu**[2] | **Weijie Zhong**[1] | **Yi Li**[1] | **Wenchuan Zhang**[1] ⓘ

[1]Department of Neurosurgery, Shanghai Ninth People's Hospital, Shanghai Jiao Tong University School of Medicine, Shanghai, China

[2]Department of Ultrasound, Shanghai General Hospital, Shanghai Jiao Tong University School of Medicine, Shanghai, China

Correspondence
Wenchuan Zhang and Yi Li, Department of Neurosurgery, Shanghai Ninth People's Hospital, Shanghai Jiao Tong University School of Medicine, No. 639 Zhizaoju Road, Shanghai 200011, China.
Email: zhangwench88@sjtu.edu.cn and snailliyi@163.com

Abstract

Cerebral ischemia–reperfusion (I/R) injury as the consequence of revascularization after ischemic stroke is associated with mitochondrial dysfunction, oxidative stress, and neuron loss. In this study, we used a deprivation/reoxygenation (OGD/R) model to determine whether interactions between Netrin-1, AKT, and the mitochondrial AAA protease AFG3L2 could influence mitochondrial function in neurons after I/R. We found that Netrin-1 protects primary cortical neurons from OGD/R-induced cell death and regulates mitochondrial reactive oxygen species (ROS) and Ca^{2+} levels. The accumulation of mitochondrial calcium uniporter (MCU) subunits was monitored in cells by immunoblot analysis. Although the regulatory subunits MICU1 and MICU2 were relatively unaffected, the accumulation of the essential MCU regulator (EMRE) subunit was impaired. In OGD/R-induced cells, the 7 kDa form of EMRE was significantly reduced. Netrin-1 inhibited the accumulation of EMRE and mitochondrial Ca^{2+} levels by upregulating AFG3L2 and AKT activation. Loss of AFG3L2 or inhibition of AKT increased levels of 7 kDa EMRE. Moreover, overexpression of AKT increased the expression of AFG3L2 in Netrin-1-knockdown neurons after OGD/R. Our results demonstrate that Netrin-1 enhanced AFG3L2 protein expression via activation of AKT. We also observed that overexpression of Netrin-1 significantly reduced infarction size in an I/R-induced brain injury model in rats but not when AKT was inhibited. Our data suggest that AFG3L2 is a protein substrate of AKT and indicate that Netrin-1 attenuates cerebral I/R injury by limiting mitochondrial ROS and Ca^{2+} levels through activating AKT phosphorylation and AFG3L2.

Abbreviations: AFG3L2, ATPase family gene 3-like 2; CHX, cycloheximide; FITC, fluorescein isothiocyanate; I/R, ischemia-reperfusion; LDH, lactate dehydrogenase; MCAO, middle cerebral artery occlusion; MCU, mitochondrial calcium uniporter; MDA, malondialdehyde; OGD/R, oxygen–glucose deprivation and reperfusion; PI, propidium iodide; ROS, reactive oxygen species; SOD, superoxide dismutase; TUNEL, terminal deoxynucleotidyl transferase dUTP nick end labeling.

Xiaosheng Yang, Yang Liu, and Weijie Zhong contributed equally to this work.

1 | INTRODUCTION

Cerebral ischemia–reperfusion (I/R) injury as the consequence of revascularization after ischemic stroke can be accompanied by mitochondrial dysfunction, oxidative stress, and the loss of neurons.[1,2] The high energy demand of cerebral tissues is fulfilled by mitochondrial oxidative phosphorylation with high levels of reactive oxygen species (ROS) generated as a by-product.[3] Therefore, mitochondrial dynamics play an important role in maintaining the stability of cells and the size of the infarct area after I/R injury.[4,5]

Obstruction of the blood supply by I/R leads to reduced levels of ATP and elevated levels of mitochondrial Ca^{2+}.[6] High levels of intracellular Ca^{2+} can predispose cells to mitochondrial failure and apoptotic death. The mitochondrial calcium uniporter (MCU) and essential MCU regulator (EMRE) are both involved in the regulation of mitochondrial Ca^{2+} levels.[7] The upregulation of MCU can increase mitochondrial fission, the inhibition of mitochondrial fusion, and mitophagy in a mouse I/R model, whereas the suppression of MCU can reduce infarction area and restore mitochondrial function.[8]

Along with slits, ephrins, and semaphorins, netrins are axon guidance factors that play a prominent role in the formation of the nervous system.[9] Netrin-1 is differentially regulated after nerve injury and is thought to participate in peripheral nerve regeneration.[10] Netrin-1 is also known to attenuate hypoxia-driven inflammation[11,12] and alleviate myocardial I/R injury.[13,14] Moreover, following cerebral stroke, Netrin-1 can reduce infarct size in rats through the inhibition of Notch signaling[15] and was found to protect neurons from apoptosis by activating the ERK signaling pathway.[16] However, whether other pathways are activated or inhibited by Netrin-1 in response to I/R injury is unclear.

Accumulative evidence indicates that the neuroprotective kinase AKT (also known as protein kinase B) is involved in stroke progression.[17] Following cerebral I/R injury, activation of AKT mediates neuronal survival, apoptosis, oxidative stress, calcium overload, and mitochondrial dysfunction.[18–20] AKT is known to interact with Netrin-1 in hypoxic microenvironments and Netrin-1 increases the levels of p-AKT in primary cultured astrocytes.[21,22]

ATPase family gene 3-like 2 (AFG3L2) is an m-AAA protease that is involved in respiratory chain activity and the regulation of mitochondrial gene expression.[23]

Previous studies have shown that the loss of m-AAA protease results in the accumulation of MCU-EMRE channels lacking gatekeeper subunits in neuronal mitochondria, which results in mitochondrial Ca^{2+} overload, mitochondrial permeability transition pore opening, and eventually neuronal death.[24] In this study, we examined the roles of Netrin-1, the AKT pathway, and AFG3L2 after I/R injury using oxygen–glucose deprivation and reperfusion (OGD/R) in neurons in vitro and a middle cerebral artery occlusion (MCAO) model in rats. In particular, we studied the effects of differential expression on the regulation of mitochondrial Ca^{2+} levels by MCU and EMRE. Our findings contribute to a better understanding of Ca^{2+} overload in the loss of neurons and may assist in the therapeutic management of cerebral stroke.

2 | MATERIALS AND METHODS

2.1 | Antibodies and reagents

Antibodies to Netrin-1 (1 μg/mL), NeuN (5 μg/mL) and AFG3L2 (5 μg/mL) were from Abcam (Cambridge, UK). AKT consensus phosphorylation sequence RXXpS/pT, p-AKT (Ser473, western blotting, 1:1000; immunofluorescence, 1:100), and AKT (1:1000) were from Cell Signaling (Danvers, MA, USA). GST tag (1:1000) and HA tag (1:500) were from GeneTex (Irvine, CA, USA). FLAG (1:5000) was from Thermo Fisher Scientific (Waltham, MA, USA), β-actin was from (1:1000) Santa Cruz (Dallas, TX, USA), and COX2 (subunit of Complex IV, 1:1000) was from Abcam. Alexa Fluor® 647-conjugated rabbit anti-NeuN (1:50), Alexa Fluor 647-conjugated goat anti-mouse IgG (1:200), and Alexa Fluor488-conjugated goat anti-rabbit IgG (1:200) were from Abcam. For immunofluorescence experiments, Rhod-2 AM, fluorescent Ca^{2+} indicator was from Abcam; MitoTracker Green was from Beyotime (Shanghai, China); MitoSOX Red and Cycloheximide (CHX) were from Sigma-Aldrich (St. Louis, MO, USA). The small molecule AKT inhibitor, MK2206, was from SelleckChem (Houston, TX, USA).

2.2 | Cell cultures

Primary neuronal cells were derived from neonatal Sprague–Dawley (SD) rats as described previously.[20] Briefly, rat cortical tissues were isolated from embryonal

rat brains (aged 16–18 days) and maintained in ice-cold phosphate-buffered saline (PBS). The tissue was digested using 0.25% trypsin (Gibco, Waltham, MA, USA) for 10 min at 37°C and then the cells were dispersed in Dulbecco's modified Eagle medium (DMEM)/F12 (Gibco) containing 10% fetal bovine serum (FBS) followed by centrifugation at 200 g for 5 min at 4°C. Following centrifugation, cells were resuspended in DMEM/F12 medium and seeded onto poly-D-lysine coated plates. Cells were seeded at a density of 5×10^4–1×10^6 cells/well and maintained at 37°C and 5% CO_2 for 4 h before the replacement of media with serum-free neurobasal-A media containing 2% B27 (Gibco).

2.3 | Oxygen–glucose deprivation and reperfusion (OGD/R) model

The OGD/R model was developed as described previously with minor modifications.[20] The primary cells were cultured in the presence of glucose and serum-free medium and incubated in an anaerobic chamber, which contained 5% CO_2 and 95% N_2 at 37°C. After 2 h, the cells were transferred to normal growth culture medium and continued to be cultured under normal conditions for 24 h.

2.4 | Adenovirus, plasmids, and gene silencing

Adenoviral particles overexpressing Netrin-1 (rat) and the mock plasmid pUC57 were purchased from Vigene Biosciences (Shandong, China). The adenovirus targeting Netrin-1 (Ad-shNetrin-1) and non-specific negative control (Ad-shControl) were also purchased from Vigene Biosciences. Four 19-nt siRNAs targeting different nucleotide sites of Netrin-1 mRNA were designed, and four pairs of 57-nt oligonucleotides coding shRNAs containing 19-nt reverted repeat, 9-nt spacer sequence, and BamHI and HindIII restriction enzyme sites were synthesized. Oligonucleotides were annealed and inserted into the shRNA expression vector pAdM-shRNA-GFP to form pAdM-shRNA-GFP Netrin-1-shRNA1-4. The following oligonucleotides were used in gene silencing.

Netrin-1 shRNA1: 5′-GCAACTCTTCCGATCCCAAGATT CAAGAGATCTTGGGATCGGAAGAGTTGCTTTTTT-3′. Netrin-1 shRNA2: 5′-GGTGCCCTTCCAATTCTATTCTT CAAGAGAGAATAGAATTGGAAGGGCACCTTTTTT-3′. Netrin-1 shRNA3: 5′-GCTTGCAAAGCCTGTGATTGCTT CAAGAGAGCAATCACAGGCTTTGCAAGCTTTTTT-3′. Netrin-1 shRNA4: 5′-GGTAAGACCTGCAATCAAACCTT CAAGAGAGGTTTGATTGCAGGTCTTACCTTTTTT-3′.

Purified recombinant Ad plasmid DNA was used to transfect the adenovirus packaging cell line (HEK293

cells). Recombinant adenoviruses were typically generated within 7 to 12 days. Transfected cells were collected, lysed through freeze–thaw cycles, and centrifuged to remove cellular debris. The supernatant was then used for large-scale virus preparation.

For AFG3L2 knockdown, the shRNA expression vector containing AFG3L2 shRNA was constructed using pGPU6/GFP/Neo by GenePharma Co. (Shanghai, China). For negative control, the shRNA was randomly scrambled. The negative control shRNA (shNC) sequences were as follows: 5′-CACCGTTCTCCGAACGTGTCACGTTCAAG AGATTACGTGACACGTTCGGAGAATTTTTTG-3′.

AKT cDNA was PCR-amplified and cloned into a pCMV-C-HA (Beyotime) expression vector to generate an HA-tagged AKT expression vector. AFG3L2 cDNA was PCR-amplified and cloned into and pCMV-C-Flag (Beyotime) expression vector to generate a FLAG-tagged AFG3L2 expression vector. For recombinant protein purification, rat AFG3L2 cDNA was amplified by PCR and cloned into a pGEX4T-1 expression vector to generate a GST-tagged AFG3L2 expression vector.

2.5 | Quantitative PCR (qPCR)

TRIzol reagent was used to extract total RNA from cultured neurons using the manufacturer's guidelines. RNA was reverse-transcribed, and qPCR was performed using an SYBR Green I PCR kit (Takara, Shiga, Japan) following the manufacturer's instructions. Each sample was normalized using β-actin. The qPCR was performed in triplicate and was normalized to β-actin expression. The qPCR conditions used were 95°C for 10 min followed by 45 cycles of 95°C for 10 s, 63°C for 5 s, and 72°C for 15 s. Gene expression was analyzed using the $2^{-\Delta\Delta CT}$ method relative to the expression of the reference gene β-actin. All experiments were repeated three times independently.

2.6 | Cell viability assessment

The viability of cells was assessed using a lactate dehydrogenase (LDH) leakage assay following the instruction of an LDH assay kit (Beyotime, China). The assay measures the loss of membrane integrity after the transformation of NADH into NAD indicated by lower levels of LDH activity at 340 nm. The experiment was repeated at least three times.

2.7 | Flow cytometry

Flow cytometry was used to detect the apoptosis rates of neurons using the Annexin V-fluorescein isothiocyanate

(FITC)/propidium iodide (PI) double staining apoptosis detection kit (BD Biosciences Pharmingen, San Jose, CA, USA). In brief, 24 h after OGD, neurons were stained with Annexin V/PI following the manufacturer's instructions. After washing the neurons with PBS at 4°C, they were resuspended in incubation buffer (200 μL) followed by Annexin V-FITC labeling reagent (5 μL) and then the neurons were incubated in the dark at room temperature for 15 min, followed by the addition of 5 μL of PI and 200 μL of binding buffer. Finally, the stained apoptotic cells were identified by the FACSCanto II system (BD Bioscience, USA), and the data were analyzed using the FlowJo software. The percentage of apoptotic cells was expressed as a percentage of the total number of early apoptotic (Annexin V-FITC positive/PI negative) and late apoptotic/necrotic cells (Annexin V-FITC positive/PI positive). The experiment was repeated three times.

2.8 | Immunofluorescence and TUNEL assay

A terminal deoxynucleotidyl transferase dUTP nick end labeling (TUNEL) assay was conducted using a One Step TUNEL Apoptosis Assay Kit purchased from Beyotime (Shanghai, China) according to the manufacturer's instructions. Images were obtained using a fluorescence microscope (Olympus BX53, Japan). The apoptosis rate (%) was calculated as the percentage of TUNEL-positive cells to the total number of cells.

2.9 | Mitochondria isolation

To isolate mitochondria, cells were suspended in homogenizer buffer (220 mM mannitol, 70 mM sucrose, 5 mM HEPES/KOH pH 7.6, and 0.2% BSA) and homogenized. The mitochondria were separated from the homogenized cell suspension by differential centrifugation. This process was repeated three times.

2.10 | Western blot analyses

Cell extracts were obtained from neurons by using RIPA lysis buffer (Beyotime, China). Protein concentration was determined using a Pierce BCA Protein Assay Kit (Thermo Fisher Scientific). Equal amounts of protein were separated by SDS-PAGE and then transferred to PVDF membranes. Membranes were blocked with blocking solution (Beyotime) for an hour and then incubated with primary antibodies (Section 2.1) overnight at 4°C. After washing

thoroughly in PBS with 1% Tween, the membranes were incubated with goat anti-rabbit IgG-HRP secondary antibody at room temperature for an hour. ECL reagent was used to visualize the immunoreactive bands and ImageJ software was used to measure band intensity.

2.11 | Measurement of mitochondrial ROS levels

To measure mitochondrial ROS, cells were co-stained with MitoSOX Red mitochondrial superoxide indicator (Sigma-Aldrich, 5 μM) as described previously.[25] After washing with PBS, cells were analyzed with an Olympus BX53 fluorescence microscope (excitation at 480–550 nm, emission at 590 nm). Each experiment was repeated three times.

2.12 | Confocal imaging of mitochondrial Ca^{2+}

Confocal imaging of mitochondrial Ca^{2+} was performed with Rhod-2/AM (Abcam) and MitoTracker Green as described previously.[26] Briefly, cells were incubated with Rhod-2/AM and MitoTracker Green for 30 min on a coverslip. Tyrode's solution was added and the cells were incubated again for 30 min at room temperature protected from light. Confocal Imaging of the Mitochondrial Rhod-2/AM and MitoTracker Green Fluorescence-loaded cells was performed in phase contrast at 40×. Cell membranes were permeabilized with permeabilization solution (100 mM potassium acetate, 15 mM KCl, 5 mM KH$_2$PO$_4$, 5 mM Mg-ATP, 0.35 mM EGTA, 0.12 mM CaCl$_2$, 0.75 mM MgCl$_2$, 10 mM phosphocreatine, 10 mM HEPES, and pH 7.2, 0.005% saponin) to remove Rhod-2 localized to the cytosol. The permeabilization solution was then replaced with Ca^{2+} solution (100 mM potassium acetate, 15 mM KCl, 0.35 mM EGTA, 0.75 mM MgCl$_2$, 10 mM HEPES, pH 7.2). Rhod-2 fluorescence (excitation 559 nm, emission 575–675 nm) and MitoTracker green fluorescence (excitation 488 nm, emission 505–525 nm) were measured with an Olympus confocal microscope.

2.13 | In vitro kinase activity assay

GST-tagged AFG3L2 was purified from *E. coli* and quantified using a Bradford assay. Then, GST-tagged AFG3L2 (1 μg) was incubated with an increasing amount of active full-length recombinant AKT protein in kinase buffer containing 25 μM unlabeled ATP and 2.5 μCi of γ-[^{32}P]-ATP. The assay mixtures were incubated at 30°C for 30 min. The reactions were stopped by adding an equal volume

of 2× SDS loading buffer and heated to 95°C for 5 min. Samples were then separated by 8% SDS-PAGE, transferred onto nitrocellulose membranes, and measured by autoradiography.

2.14 | Cycloheximide chase assay

Cells were transfected with an AFG3L2 expression construct for 24 h and then treated with protein synthesis inhibitor CHX (20 μg/mL) for the times indicated. Protein lysates were harvested at the indicated time points and protein abundances were analyzed by immunoblotting analysis using antibodies (Section 2.1).

2.15 | Animals, MCAO model, and animal grouping

All experimental procedures were approved by the Animal Welfare and Use Committee of Shanghai Jiaotong University (Ethical approval number: SH9H-2019-A529-1) in accordance with the NIH Guide for the Care and Use of Laboratory Animals. Approximately 60 adult male SD rats (6–8 weeks old, 280 to 300 g) were used in the experiments. All rats were housed in a light and temperature-controlled room with free access to food and water.

The MCAO model of I/R was created in rats as described previously.[27,28] Briefly, rats were first anesthetized by intraperitoneal injection of chlorine hydrate (10%, 400 mg/kg). The left common carotid artery (CCA), external carotid artery (ECA), and internal carotid artery (ICA) were revealed. The proximal ends of ECA and CCA were ligated with nylon monofilament. The distal end of the CCA was also secured. A small incision was cut in the CCA and a nylon monofilament was inserted into the ICA for 2 h. After 2 h, the nylon monofilament was withdrawn. The sham group received the same surgical procedure without obstructing blood flow. After awakening, the rats were maintained in cages with free access to food and water for 12 h.

Sixty male SD rats were randomly divided into six groups as follows: (1) sham, (2) MCAO+AAV-Ctrl (Adeno-associated virus control vectors), (3) MCAO+AAV-Netrin-1, (4) MCAO+AAV-Netrin-1 +MK2206, (5) MCAO+ AAV-shControl, and (6) MCAO+AAV-shNetrin-1. In the sham group, the rats were injected with 0.9% normal saline and were not subjected to MCAO. The pAV-FH control vector, pAV-Netrin-1, pAV-U6-shControl, and pAV-U6-shNetrin-1 were purchased from Vigene Biosciences (Shandong, China). A burr hole was drilled into the pericranium. A 10-ml syringe was inserted into the basal ganglia 3 mm under the meninges. AAV vectors were injected into the hemisphere 90 min before the MCAO. MK2206, an AKT inhibitor, dissolved in DMSO was injected 30 min before the MCAO using the same procedure.

2.16 | Neurological function scores

The neurological function score was evaluated by a blinded investigator at 72 h after MCAO surgery using Zea longa's 5-point scale system.[27]

2.17 | Measurement of cerebral infarction volume

After the neurological function score was completed, three rats were randomly selected from each group to measure their cerebral infarction volumes. Infarct volume was measured immediately after the removal of brains from the rats. Brains were sectioned coronally into 2-mm slices and incubated with 2% 2,3,5 triphenyltetrazolium chloride (TTC, Sigma-Aldrich) for 15 min. The infarct area was determined from the total hemispheric area using ImageJ.

2.18 | Immunofluorescence staining

Double immunofluorescence staining was performed as previously described.[29] Briefly, after decapitation, the brains were removed immediately, immersed into pre-chilled isopentane, and placed inside a −80°C refrigerator for 10 min for snap-freezing. Then, the brains were embedded in optimum cutting temperature compound (Sakura Finetek Inc., Torance, CA, United States) and stored in the −80°C refrigerator. Brains were cut into 10-μm-thick coronal sections, were fixed with 4% paraformaldehyde at room temperature for 15 min, and washed three times with PBS. After permeabilization with 1% Triton X-100 for 10 min, the sections were blocked with 10% goat serum in PBS for 1 h. Subsequently, the sections were incubated at 4°C overnight with primary antibodies: mouse anti-NeuN, rabbit anti-p-AKT, and rabbit anti-AFG3L2 followed by incubation with appropriate fluorescence-conjugated secondary antibodies for 1 h at room temperature were then incubated with DAPI for 5 min. The sections were visualized and photographed with an Olympus BX53 fluorescence microscope.

For double staining of TUNEL and the markers of neuron NeuN, Alexa Fluor® 647-conjugated rabbit anti-NeuN antibody, combined with TUNEL staining, was selected to assess the apoptosis of neuron cells. The apoptosis rate (%) was calculated as the percentage of TUNEL-positive cells to the number of neuron cells.

2.19 | Statistical analysis

All data were analyzed using GraphPad Prism (GraphPad Software, San Diego, CA, USA). One-way analysis of variance (ANOVA) was used to measure statistical differences between groups and post hoc Tukey tests were used for multiple comparisons. Data were expressed as mean $\pm$ standard deviation (SD) unless otherwise stated and a p-value $<.05$ was considered statistically significant.

3 | RESULTS

3.1 | Netrin-1 protects primary cortical neurons from OGD/R-induced cell death and apoptosis

Initially, we observed that OGD/R significantly elevates Netrin-1 mRNA levels in primary cortical neurons. To further understand its downstream consequences, we silenced or overexpressed Netrin-1 (Figure 1A).
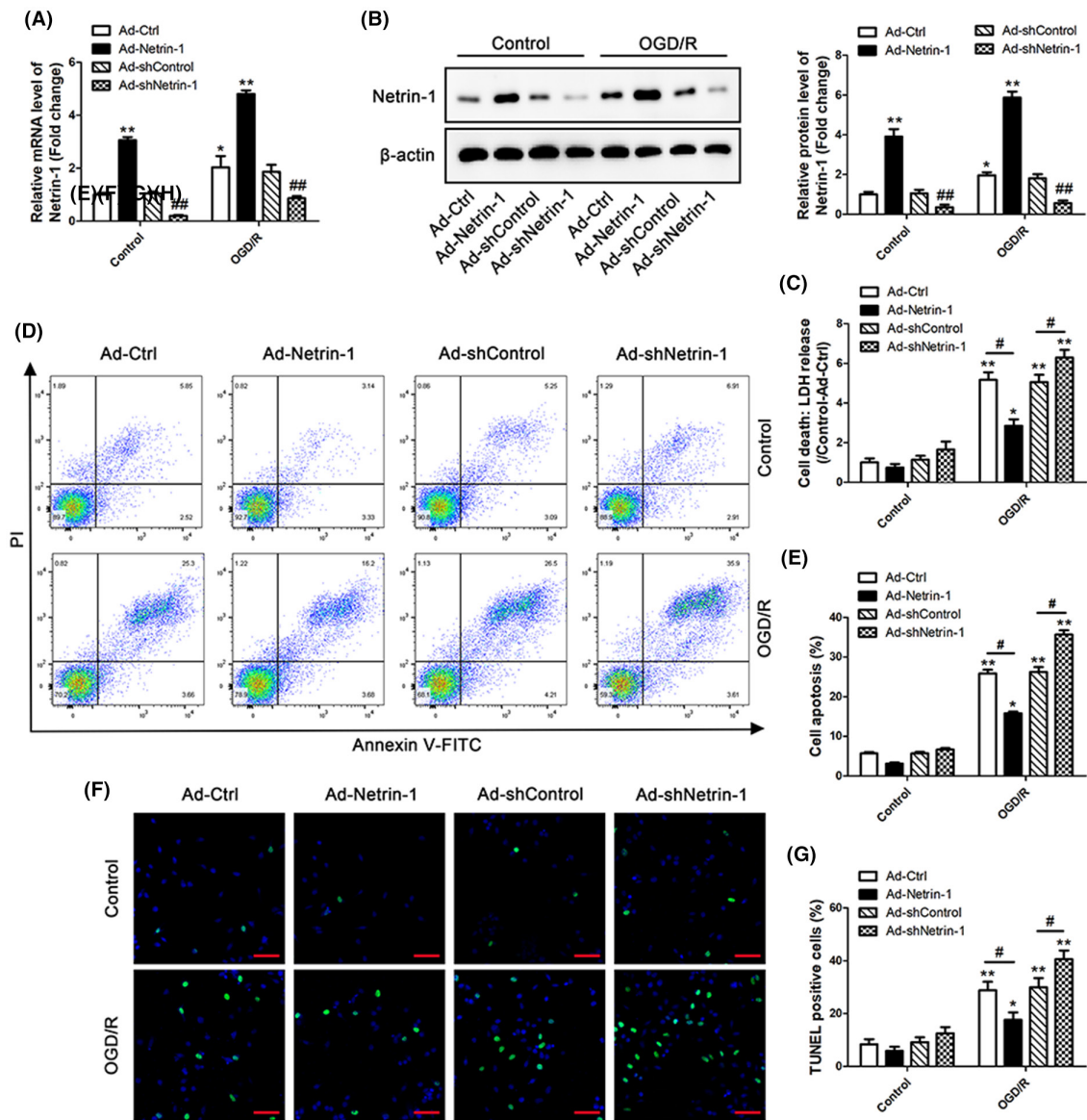

FIGURE 1 Netrin-1 regulates OGD-induced neuronal cell death and apoptosis. (A, B) The overexpression or knockdown of Netrin-1 adenovirus transfected into primary cortical neurons. The mRNA (A) and protein (B) expression levels of Netrin-1 24 h after oxygen–glucose deprivation (OGD) were detected by RT-PCR and western blot analysis. *vs. the Ad-Ctr group, #vs. the Ad-shControl group. (C) Cell death rates of each group were measured by lactate dehydrogenase (LDH) release. *vs. the Control group. (D) Apoptosis was detected by flow cytometry. The signals detected in Q2 and Q4 quadrants represent the apoptotic neurons. (E) Quantification and graphical representation of the flow cytometry results. *vs. control group. (F) Representative images of TUNEL (green)-positive neurons. The scale bars represent 100 μm. (G) Quantification of TUNEL-positive neurons for the indicated conditions. *vs. control group. *, #$p < .05$, **, ##$p < .01$.

Downregulation or upregulation of Netrin-1 after genetic modifications was further confirmed using western blotting analysis (Figure 1B). A lactate dehydrogenase (LDH) release assay indicated that exposure to OGD/R significantly increased LDH release which corresponds to higher cell death in primary cortical neurons. However, overexpression of Netrin-1 significantly decreased cell death in these cells. Downregulation of Netrin-1 further exacerbated OGD/R-induced cell death, compared to controls (Figure 1C). Flow cytometric analysis also indicated a significant increase in the percentage of apoptotic neuronal cells postexposure to OGD/R. However, overexpression of Netrin-1 significantly decreased apoptotic cells, whereas the downregulation of Netrin-1 resulted in the opposite effect (Figure 1D,E). These results were confirmed using a TUNEL assay (Figure 1F,G) and indicated that the upregulation of Netrin-1 protected cortical neurons against OGD/R-induced cell death and apoptosis.

3.2 | Netrin-1 regulates OGD/R-induced mitochondrial ROS and Ca^{2+} levels in neurons

Since OGD/R is known to induce mitochondrial ROS in cells, we wanted to understand the role of Netrin-1 in this process. We used red mitochondrial superoxide indicator (MitoSOX Red) to assess the levels of mitochondrial ROS in cells exposed to OGD/R. Silencing of Netrin-1 post-OGD/R significantly increased mitochondrial ROS levels, whereas overexpression did the reverse (Figure 2A,B). To assess the changes in mitochondrial Ca^{2+} levels after exposure to OGD/R, we co-stained cells with mito-tracker and rhod-2, a Ca^{2+} indicator. It was clear that OGD/R significantly increased mitochondrial Ca^{2+} levels, which could be mitigated by Netrin-1 overexpression. However, silencing of Netrin-1 significantly increased the effect of OGD/R on mitochondrial Ca^{2+} levels (Figure 2C,D). We monitored the accumulation of MCU subunits in cells by western blot analysis. The levels of MCU regulatory subunits, mitochondrial calcium uptake 1 and 2 (MICU1 and MICU2), were only moderately affected postexposure to OGD/R (Figure 2E,F). In contrast, the levels of the MCU subunit EMRE in cells were severely impaired. Two forms of the subunit were detected at 7 and 11 kDa. In both the control and OGD/R exposed cells, levels of the 11 kDa premature subunit remained unchanged. However, we observed significantly reduced levels of the 7 kDa form of mature EMRE subunit in OGD/R exposed cells (Figure 2E,F). Netrin-1 overexpression facilitated an increase in the accumulation of the mature EMRE subunit; however, the knockdown of Netrin-1 further decreased the level of the mature EMRE subunit in OGD/R-induced neurons (Figure 2E,F).

3.3 | Netrin-1 acts via upregulation of AFG3L2 and AKT activation in OGD/R-induced neuron

Previous studies have shown that mitochondrial Ca^{2+} overload results from the loss of m-AAA protease and the accumulation of constitutively active MCU-EMRE. In addition, the activation of AKT is involved in neuronal survival, apoptosis, oxidative stress, calcium overload, and mitochondrial dysfunction following cerebral I/R injury. To clarify the involvement of m-AAA proteases and AKT signaling in I/R injury, we first measured the levels of AFG3L2 protein and AKT signaling by western blotting. It was evident that exposure to OGD/R decreased AFG3L2 protein levels and phosphorylated AKT (p-AKT) levels (Figure 3A,B). Additionally, we could observe that the overexpression of Netrin-1 reversed this effect. However, silencing Netrin-1 exacerbated the effects of OGD/R as indicated by the decreased levels of AFG3L2 and p-AKT (Figure 3A,B). In addition, we assessed the EMRE levels and observed that overexpression of Netrin-1 under OGD/R exposure significantly increased mature EMRE levels, which was rescued by the silencing of AFG3L2 and inhibition of AKT. And the levels of MCU, MICU1, and MICU2 in OGD/R-induced neuron were not affected by Netrin-1 overexpression, silencing of AFG3L2, and inhibition of AKT. These results indicated that AFG3L2 and AKT signaling may be involved in the neuroprotective effects of Netrin-1 (Figure 3C,D). Importantly, silencing of AFG3L2 and inhibition of AKT in the Netrin-1-overexpression neurons also significantly increased neuronal mitochondrial Ca^{2+} levels (Figure 3E,F).

3.4 | AKT phosphorylates AFG3L2 and promotes AFG3L2 stability

AKT has been identified to be a neuroprotective agent that phosphorylates its downstream target proteins thereby playing an essential role in stroke progression. Hence, we assessed whether AKT signaling regulated Netrin-1-induced AFG3L2 protein expression in neurons after OGD/R. Initially, we performed western blotting and found that overexpression of Netrin-1 upregulated AFG3L2 protein expression. Using AKT inhibitor MK2206, we could demonstrate that AFG3L2 protein expression could be significantly suppressed. Overexpression of AKT increased the expression of AFG3L2 in Netrin-1-knockdown neurons after OGD/R (Figure 4A). These results clearly
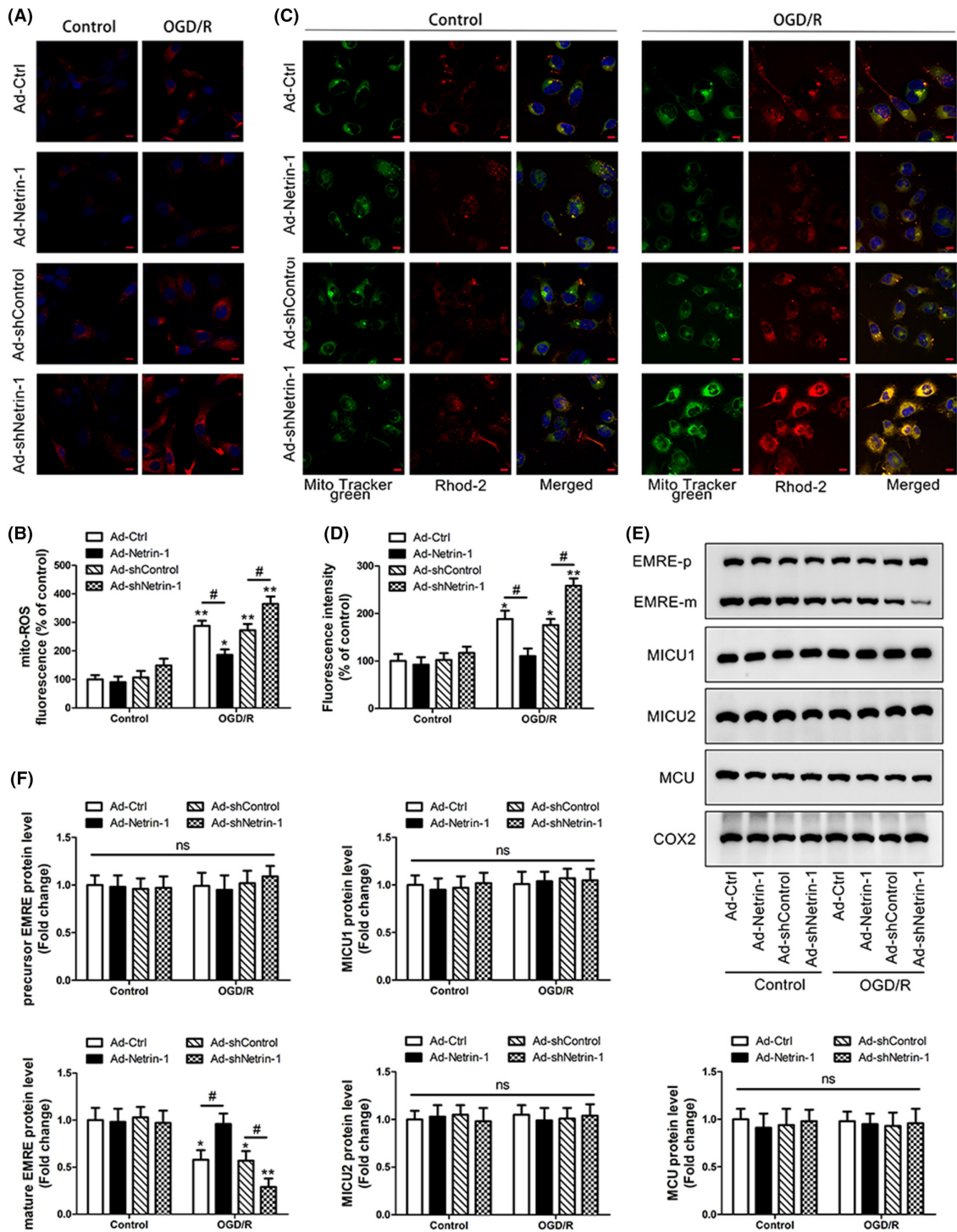
FIGURE 2 Netrin-1 regulates OGD/R-induced mitochondrial ROS and Ca^{2+} levels in neurons. (A) Mitochondrial ROS levels in each group were measured by staining the cells with MitoSOX Red and imaged using fluorescence microscopy. Scale bar 10 μm. (B) Relative fluorescence intensity of ROS was detected. *$p < .05$, **$p < .01$, compared with the control. (C) Representative fluorescence images of primary cortical neurons loaded with both rhod-2 (red) and MitoTracker green (green) and merged images of the two dyes (yellow) after oxygen–glucose deprivation (OGD) with respective controls. Scale bar 10 μm. (D) Mean fluorescent intensities of Rhod-2 and MitoTracker green (yellow) show the mitochondrial Ca^{2+} levels in each group. (E) The mitochondrial calcium uniporter (MCU) complex and the regulatory subunits MICU1 and MICU2, EMRE levels were analyzed in neuron mitochondria using western blotting. (F) Quantification of the precursor [p] and mature [m] EMRE subunits (SD; $n = 3$). COX2 serves as a mitochondrial loading control. *vs. control group. *,#$p < .05$, **$p < .01$.
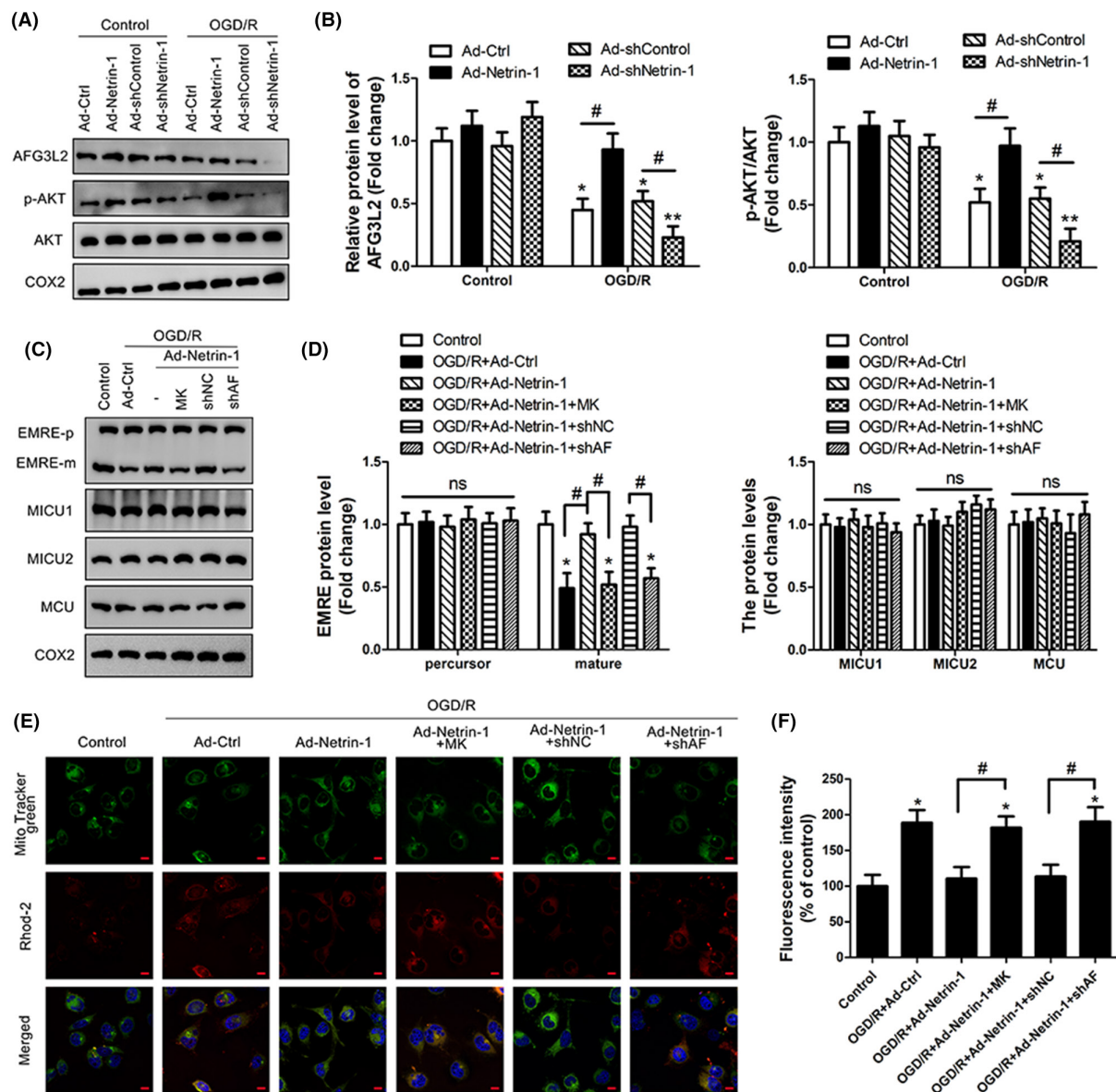
FIGURE 3 Netrin-1 acts via upregulation of AFG3L2 and AKT activation in OGD/R-induced neurons. (A) Western blot analysis of AFG3L2, p-AKT, and AKT expression in isolated mitochondria from primary cortical control and OGD/R-induced neurons with Netrin-1 overexpressed or knocked down. COX2 served as a mitochondrial loading control. (B) Quantification of the expression through assessment of band intensity. (C) Primary cortical control and OGD/R-induced neurons were transfected with either an empty vector (Ad-Ctrl) or Netrin-1 adenovirus overexpression system (Ad-Netrin-1) and exposed to the AKT inhibitor MK2206 (MK), shNC, or sh-AFG3L2 (shAF). The steady-state level of EMRE in primary cortical control and OGD/R-induced neuronal mitochondria transfected with the indicated constructs. The level of precursor [p] EMRE was quantified. COX2 served as a mitochondrial loading control. (D) Quantification of the expression through assessment of band intensity. (E) Representative fluorescence image of these transfected cells loaded with rhod-2 (red) and MitoTracker green (green) along with merging of the two channels (yellow) after oxygen–glucose deprivation (OGD), with respective controls. Scale bar 10 μm. (F) Mean fluorescent intensities of Rhod-2 and MitoTracker green (yellow) show the mitochondrial Ca^{2+} levels in each group. *vs. control group. *,#$p < .05$, **$p < .01$.

indicated that Netrin-1 enhanced AFG3L2 protein expression via activation of AKT in neurons after OGD/R. Immunoprecipitation (IP) and reverse IP results showed that AKT interacted with AFG3L2 in neurons (Figure 4B). The substrates of AKT display a consensus motif: RXXS/T. To further identify if AKT could phosphorylate AFG3L2,

we set up a kinase assay with flag-immunoprecipitated AFG3L2 in the presence or absence of recombinant AKT and unlabeled ATP. In these experiments, the addition of AKT resulted in increased phosphorylation of AFG3L2, as detected by the AKT pS/T antibody (Figure 4C). However, when we treated neurons with a small molecule AKT
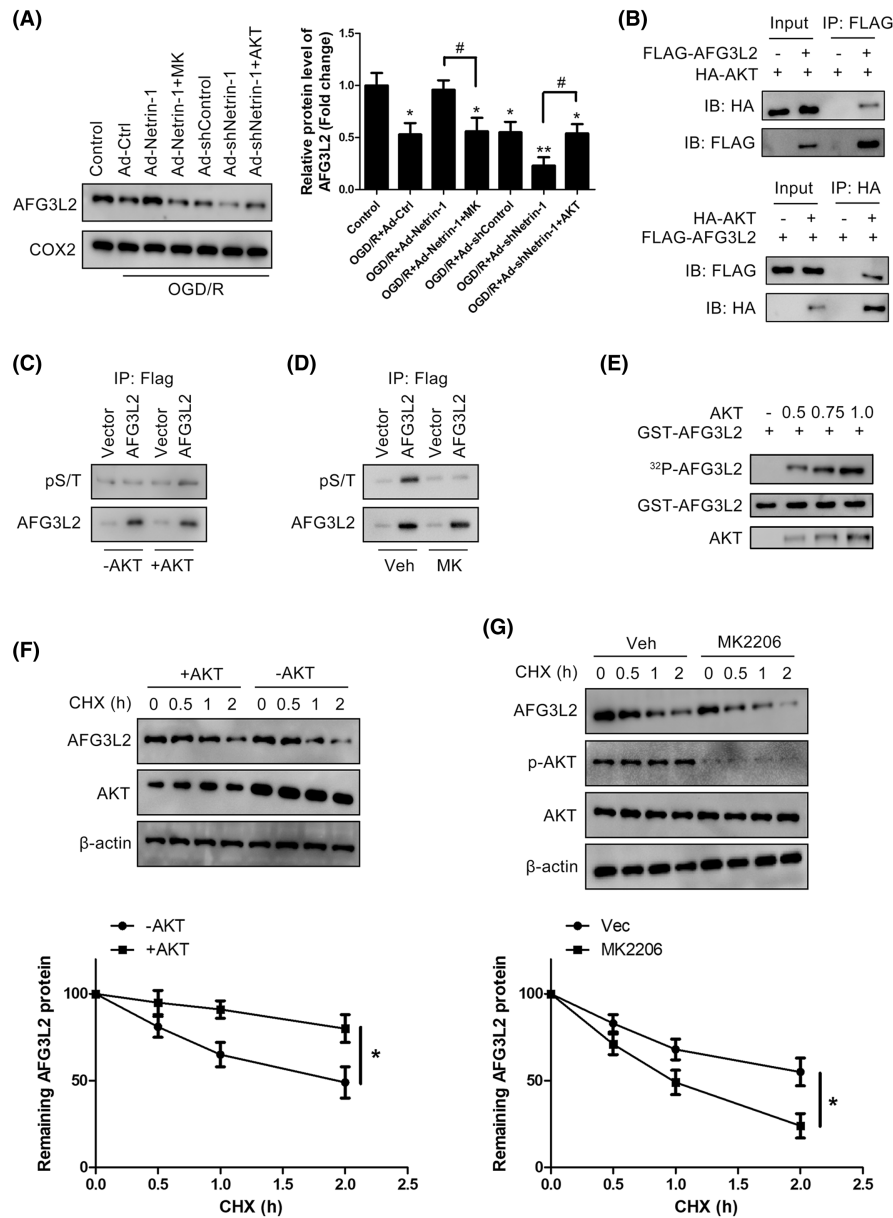
FIGURE 4 AKT phosphorylates AFG3L2 and promotes AFG3L2 stability. (A) Immunoblot analysis of mitochondrial extracts from primary cortical neurons (Control) and OGD/R-induced neurons transfected with the indicated constructs. AFG3L2 band intensity was analyzed. (B) AFG3L2 and AKT interaction were examined using immunoprecipitation (IP) western blot analysis. AFG3L2 and AKT were immunoprecipitated from total cell lysate of neurons overexpressing FLAG-tagged AFG3L2 (FLAG-AFG3L2) and/or HA-tagged AKT (HA-AKT). The pulled-down proteins were detected by anti-FLAG (up) or anti-HA (below) antibodies. (C) Proteins from primary cortical neurons transfected with either Flag-vector or Flag-AFG3L2 were immunoprecipitated with an anti-FLAG antibody and were mixed with (+) or without (−) recombinant AKT in the presence of unlabeled ATP. Western blotting analysis was performed with an AKT antibody corresponding to the consensus phosphorylation site (RXXS/T, pS/T). (D) Neurons transfected with FLAG-vector or FLAG-AFG3L2 were treated with vehicle (Veh) or small molecule AKT inhibitor, MK2206 (MK), and immunoprecipitated with an antibody against Flag and analyzed with an antibody against pS/T, by Western blotting. (E) The radioactive in vitro kinase assay demonstrated that AKT phosphorylated AFG3L2 in a dose-dependent manner. (F, G) Immunoblot analysis of cell lysates from neurons expressing AFG3L2 co-transfected with or without AKT for 24 h (G) or treated with or without AKT inhibitor MK2206 for 3 h (H) before cycloheximide (CHX, $20\,\mu g/mL$) treatment at indicated times. Percentages of the relative remaining amount of AFG3L2 are shown below the bands. AFG3L2 band intensity was normalized to β-actin and then normalized to the time = 0 of the controls.

inhibitor (MK2206), we observed reduced reactivity of immunoprecipitated AFG3L2 with the AKT pS/T antibody, compared to vehicle-treated cultures (Figure 4D). In

addition, we performed radioactive in vitro kinase assay using recombinant AKT and GST-tagged AFG3L2 in the presence of ^{32}P-γATP. We observed that AFG3L2 could

be phosphorylated by AKT in a dose-dependent manner (Figure 4E). Finally, we examined whether AKT promoted AFG3L2 protein stability. Using a cycloheximide (CHX) chase assay and showed that overexpression of AKT prolonged AFG3L2 protein half-life (Figure 4F). Conversely, inhibition of AKT activity diminished AFG3L2 protein levels (Figure 4G). These data suggest that AFG3L2 is a substrate of AKT and can be phosphorylated by AKT, thus enhancing the protein stability of AFG3L2.

3.5 | AKT inhibition or knockdown of AFG3L2 impedes the neuroprotective effects of Netrin-1 in OGD/R-induced neurons

To assess the effect of AFG3L2 and AKT on OGD/R-induced neurons, we either inhibited AKT or silenced AFG3L2. We performed TUNEL staining and observed that exposure to OGD/R significantly increased the number of TUNEL$^+$ cells (Figure 5A,D). However, overexpression of Netrin-1 reversed this effect and decreased the number of TUNEL$^+$ cells. When we inhibited AKT or silenced AFG3L2, the effect was reversed, and it appeared as if Netrin-1 could not protect the cells against OGD/R-induced apoptosis. We then assessed mitochondrial ROS levels by staining the cells with MitoSOX. After exposure to OGD/R, mitochondrial ROS levels significantly increased but could be rescued by the overexpression of Netrin-1 (Figure 5B,E). However, inhibition of AKT or AFG3L2 significantly reversed this effect as indicated by increased mitochondrial ROS levels. Similarly, we observed that exposure to OGD/R increased cell death, but this could be rescued by Netrin-1 overexpression, whereas AKT or AFG3L2 inhibition significantly reversed this effect (Figure 5C).
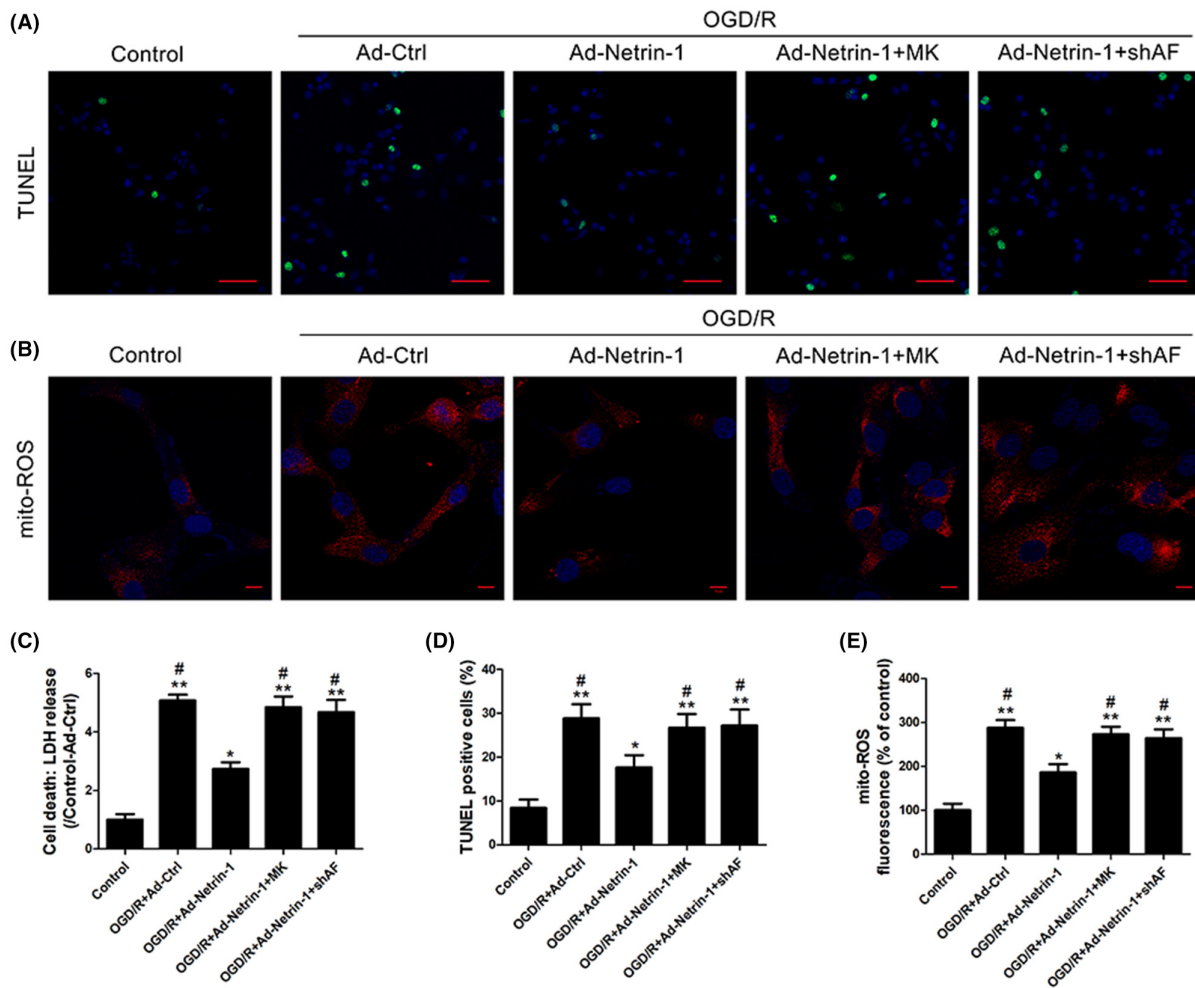

FIGURE 5 AKT inhibition or knockdown of AFG3L2 impedes the neuroprotective effects of Netrin-1 in OGD-induced neurons. (A) Representative images of TUNEL (green)-positive neurons. The scale bars represent 100 μm. (B) Mitochondrial ROS levels in each group were measured by fluorescence microscope by staining with MitoSOX Red. Scale bar 10 μm. (C) Cell death rates of each group were measured by lactate dehydrogenase (LDH) release. (D) Quantification of TUNEL-positive neurons for the indicated conditions. (E) Relative fluorescence intensity of ROS was detected. *$^{,\#}p < .05$, **$p < .01$, *vs. control group. $^{\#}$vs. OGD/R + Ad-Netrin-1 group.

3.6 | Lack of Netrin-1 and AKT inhibition exacerbates MCAO/R-induced brain injury, neurons apoptosis, and oxidative stress in rats

To clarify the role of netrin-1 in OGD/R, we developed an in vivo MCAO/R-induced brain injury model in rats.

We observed that overexpression of Netrin-1 significantly protected the rat brain as indicated by decreased infarction size compared to the respective control. The suppression of Netrin-1 resulted in a significantly high infraction size. Importantly, when AKT was inhibited, the overexpression of Netrin-1 could not protect rat brains against injury (Figure 6A,B). When we assessed
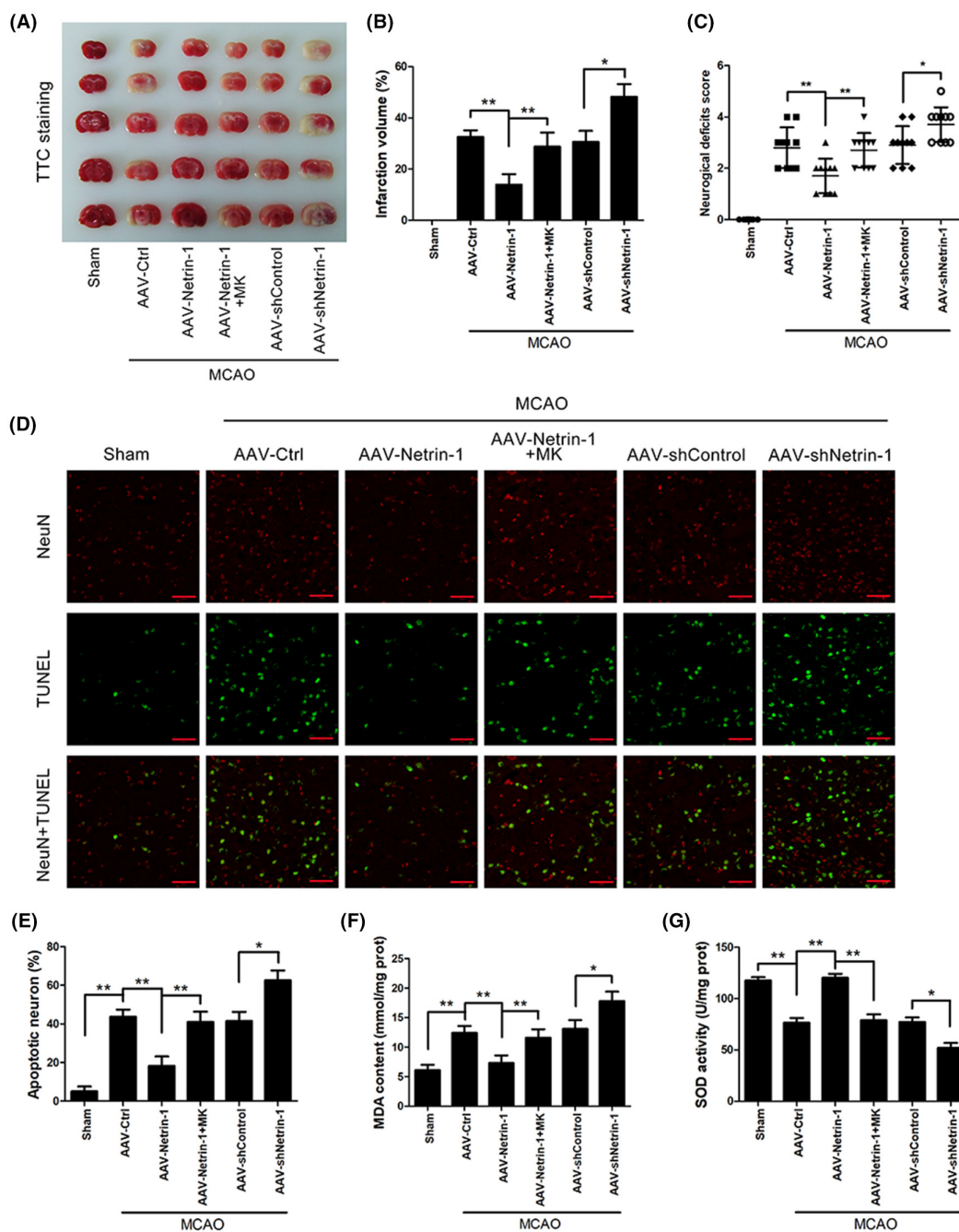

FIGURE 6 Lack of Netrin-1 and AKTinhibition exacerbated MCAO/R-induced brain injury, neuron apoptosis, and oxidative stress in rats. (A) Representative images of TTC-stained brain slices indicating brain infarction at 72 h after MCAO. (B) Quantitative analysis of infarct volumes. *$p < .05$, **$p < .01$ ($n = 5$ per group). (C) Influence of Netrin-1 on neurological scores in MCAO/R rats. ($n = 10$). (D) Effect of Netrin-1 and AKT inhibition on neuronal apoptosis in MCAO/R rats. TUNEL (green) and NeuN (red) double-stained cells (yellow) indicated apoptotic neurons. scale bar = 50 μm. (E) Quantification of apoptotic neurons in the six groups. (F) Analysis of SOD activity ($n = 5$ in each group). (G) Analysis of MDA content ($n = 5$ in each group).

neurological deficits in the MCAO rats, we observed that Netrin-1 overexpression decreased the neurological deficit score, but this was reversed in the absence of Netrin-1. However, the absence of AKT activity, even if Netrin-1 was overexpressed worsened the neurological deficit score in the MCAO rats (Figure 6C). We also ascertained that Netrin-1 overexpression decreased apoptosis and malondialdehyde (MDA) activity and increased superoxide dismutase (SOD) activity in MCAO/R injured rats (Figure 6D–G). However, the inhibition of AKT reversed this effect. These results indicated that Netrin-1 can protect the rat model against MCAO/R-induced brain injury. Interestingly, this protection by Netrin-1 is lost when AKT is inhibited in all the aforementioned experiments. Hence, it is evident that Netrin-1 confers its protection on rat brains against MCAO/R injury through the regulation of AKT activity.

3.7 | Netrin-1 activates the p-AKT/AFG3L2 pathway in MCAO/R rats

Finally, we measured the levels of Netrin-1 and AKT activity in the MCAO/R model in rats by western blotting analysis. As anticipated, the overexpression of Netrin-1 increased Netrin-1 and p-AKT levels which in turn increased AFG3L2 levels, whereas the downregulation of Netrin-1 resulted in the opposite effect. However, inhibiting AKT activity in the cells significantly decreased AFG3L2 expression levels (Figure 7A). Furthermore, we isolated mitochondria from brain tissue samples and assessed the EMRE levels. We observed that the overexpression of Netrin-1 significantly increased the levels of mature EMRE (Figure 7B). However, the inhibition of AKT reversed this effect. And the levels of MCU, MICU1, and MICU2 in MCAO/R injured rats were not affected by Netrin-1 and inhibition of AKT (Figure 7B). To confirm the role of Netrin-1 in the neuronal population, we assessed the presence of Netrin-1, p-AKT, and AFG3L2 in NeuN$^+$ neurons. As shown in Figure 7C,D, administration of AAV-Netrin-1 significantly increased the number of Netein-1$^+$ NeuN$^+$ neurons in the brain tissue of the MCAO group, while AAV-shNetrin-1 pretreatment significantly reduced the number of Netein-1$^+$ NeuN$^+$ neurons in ischemic brain tissue in rats. In the presence of Netrin-1, the tissue sections from MCAO/R rats displayed high levels of p-AKT and AFG3L2 among the NeuN$^+$ neurons. However, the use of an AKT inhibitor significantly decreased the number of NeuN$^+$ neurons expressing p-AKT and AFG3L2 (Figure 7E–H). These results indicate that Netrin-1 protects rats against MCAO/R injury by regulating the p-AKT/AFG3L2 pathway.

4 | DISCUSSION

Mitochondrial dysfunction caused by oxygen deprivation following I/R is associated with calcium overload, the generation of ROS, and neuron loss and has become the focus of therapeutic targets for ischemic stroke.[30,31] In particular, excessive Ca^{2+} leads to the activation of several calcium-dependent proteases, eventually resulting in cell death.[32,33] The accumulation of MCU and EMRE after I/R has been implicated in Ca^{2+} overload because the inhibition of MCU with ruthenium red was found to reduce total infarct volume, neuronal damage, and cell apoptosis in rats.[34] Moreover, MCU and EMRE were found to be constitutively active in neurons deficient in the m-AAA protease AFG3L2, resulting in the accumulation of Ca^{2+}.[24] Therefore, in this study, we examined whether mitochondrial Ca^{2+} overload contributed to neuronal loss in I/R injury by analyzing the regulation of MCU and EMRE by AFG3L2 and whether they are mediated by interactions between Netrin-1 and AKT.

First, we determined whether Netrin-1 could ameliorate mitochondrial dysfunction following I/R by differential expression experiments. We discovered that Netrin-1 prevented OGD/R-induced cell death in primary cortical neurons and reduced OGD/R-induced neuron mitochondrial ROS and mitochondrial Ca^{2+} levels. The neuronal protective role of Netrin-1 following OGD/R has been confirmed by other studies.[15,16] Chen et al. (2017) found that Netrin-1 could attenuate neuronal apoptosis in primary cortical neurons after OGD injury via the DCC/ERK signaling pathway and proposed that Netrin-1 could prevent DNA damage. Overexpression of Netrin-1 has also been found to regulate the Notch-1 pathway and prevent neurological damage and reduce cerebral infarct volume in rats following MCAO.[15] In addition, we found that the activation of AKT was involved in neuronal survival following OGD/R and that the inhibition of Netrin-1 could reduce the phosphorylation of AKT. Therefore, the beneficial effects of Netrin-1 overexpression in I/R injury were associated with the activation of AKT.

We also found that Netrin-1 could regulate levels of mitochondrial ROS and Ca^{2+} in neurons following OGD/R and examined levels of MCU subunits in more detail. The regulatory subunits MICU1 and MICU2 were relatively unaffected by OGD/R, but levels of the EMRE subunit were reduced. In particular, levels of the 7 kDa isoform of EMRE were significantly reduced. Netrin-1 overexpression facilitated EMRE accumulation, whereas Netrin-1 knockdown reduced the accumulation of EMRE. Therefore, our results indicate that the regulation of Ca^{2+} levels is a consequence of EMRE deficiency. We determined that this could be due to the activity of
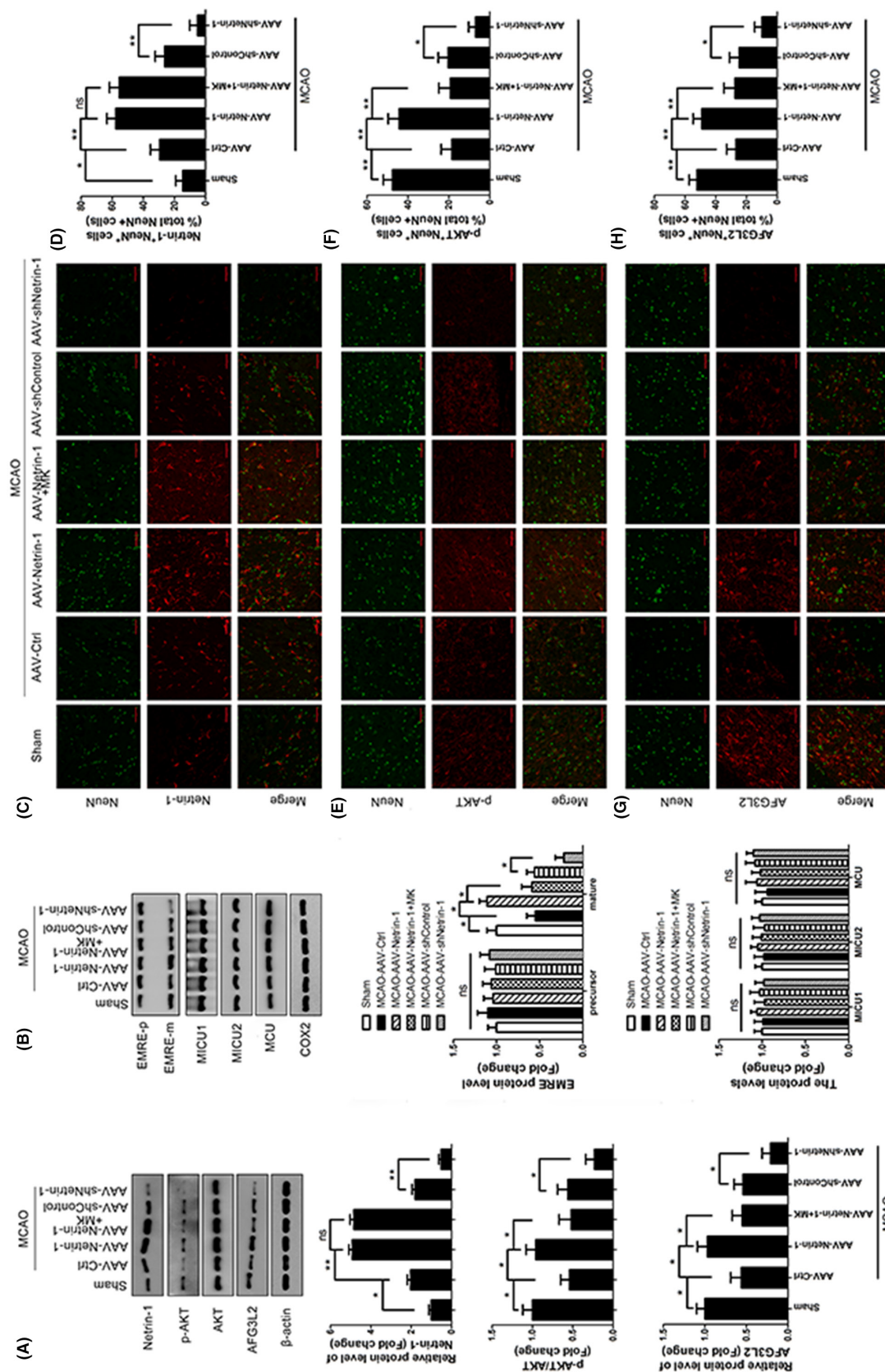
FIGURE 7 Netrin-1 activates the p-AKT/AFG3L2 pathway in MCAO/R rats. (A) Western blotting analysis of Netrin-1, p-AKT/AKT, and AFG3L2 levels in the cerebral cortex. (B) Western blot analysis of EMRE protein expression in isolated mitochondria from Sham and MCAO/R rat brains. The level of precursor [p] EMRE was quantified. COX2 served as a mitochondrial loading control. (C) Representative images of immunohistochemical staining for Netrin-1 (red) and NeuN-labeled (green) neurons in the cerebral cortex, respectively; scale bar = 50 μm. (D) Quantitative analysis of the percentage of Netrin-1-positive neurons in the cerebral cortex. (E) Representative images of immunohistochemical staining for phospho-AKT (red) and NeuN-labeled (green) neurons in the cerebral cortex, respectively; scale bar = 50 μm. (F) Quantitative analysis of the percentage of p-AKT-positive neurons in the cerebral cortex. (G) Representative images of immunohistochemical staining for AFG3L2 (red) and NeuN-labeled (green) neurons in the cerebral cortex, respectively; scale bar = 50 μm. (H) Quantitative analysis of the percentage of AFG3L2-positive neurons in the cerebral cortex.

m-AAA proteases. Other studies have suggested that Ca^{2+} accumulation could be the result of m-AAA protease deficiency.[24] König et al. (2016) reported that a neuronal interactome of m-AAA proteases in mice was responsible for regulating the subunits of MCU and Ca^{2+} overload. They discovered that m-AAA proteases regulate the assembly of MCU by degrading non-assembled EMRE.

EMRE is an integral inner membrane protein with one transmembrane domain and a predicted N-terminal mitochondrial targeting sequence facing the matrix space. König et al. (2016) reported that MAIP1 binds newly imported EMRE precursor proteins in the matrix, protects them against degradation by YME1L, and ensures their maturation by MPP. Membrane insertion of EMRE precursor proteins is accompanied by MPP-mediated maturation and assembly into MCU complexes, forming ~400 kDa complexes, which lack gatekeeper subunits, but exert Ca^{2+} channel activity (24889638). They found that the m-AAA protease AFG3L2 specifically degrades non-assembled mature EMRE independent of MAIP1 and thus modulates the formation of the ~400 kDa MCU complexes and disturbs mitochondrial Ca^{2+} handling. We also determined whether the levels of EMRE and Ca^{2+} in neurons subjected to OGD/R were influenced by the m-AAA protease AFG3L2. We discovered that the loss of AFG3L2 or the inhibition of AKT increased the levels of the 7 kDa EMRE isoform to block the inhibitory effects of Netrin-1. IP results suggested that Netrin-1 interacts with AKT and that AKT interacts with AFG3L2. Therefore, Netrin-1 enhances the expression of AFG3L2 via activation of AKT in neurons after OGD/R. The inhibition of Netrin-1 would have the opposite effect, lead to the accumulation of EMRE, and, in turn, elevate Ca^{2+} levels through AFG3L2 deficiency. It is unclear how the levels of Netrin-1 and AKT phosphorylation are inhibited by I/R injury, although it has been suggested that hypoxia-inducible factor-1a plays a key role.[35] However, several studies have found that the activation of the AKT pathway attenuates neuronal loss following I/R injury.[17,31] AKT plays a key role in preventing ROS-induced autophagy[36] and is known to be upregulated in several cancers.[37,38] Thus, although AKT activity may be detrimental in cancer, it is beneficial to the survival of neurons following I/R and could be exploited to reduce injury following I/R through regulation by Netrin-1. We confirmed the effects of overexpressing Netrin-1 after I/R in an MCAO/R model in rats. The benefits of overexpressing Netrin-1 are lost when AKT is inhibited.

To conclude, we have demonstrated that the regulation of the m-AAA protease AFG3L2 by the Netrin-1-induced activation of AKT inhibited the accumulation of EMRE and mitochondrial Ca^{2+} levels in OGD/R-induced neurons. Our results indicate that Netrin-1 attenuates cerebral I/R injury by limiting mitochondrial ROS and Ca^{2+} levels via activating AKT phosphorylation and the mitochondrial m-AAA protease AFG3L2.

DATA AVAILABILITY STATEMENT
The datasets generated for this study are available on request to the corresponding author.

ORCID
Wenchuan Zhang https://orcid.org/0000-0003-0894-6944

REFERENCES
1. Sun MS, Jin H, Sun X, et al. Free radical damage in ischemia-reperfusion injury: an obstacle in acute ischemic stroke after revascularization therapy. *Oxid Med Cell Longev.* 2018;2018:3804979.
2. Jurcau A, Simion A. Neuroinflammation in cerebral ischemia and ischemia/reperfusion injuries: from pathophysiology to therapeutic strategies. *Int J Mol Sci.* 2021;23:14.
3. Sarkar S, Chakraborty D, Bhowmik A, Ghosh MK. Cerebral ischemic stroke: cellular fate and therapeutic opportunities. *Front Biosci (Landmark Ed).* 2019;24:435-450.
4. Vongsfak J, Pratchayasakul W, Apaijai N, Vaniyapong T, Chattipakorn N, Chattipakorn SC. The alterations in mitochondrial dynamics following cerebral ischemia/reperfusion injury. *Antioxidants (Basel).* 2021;10:1384.
5. Wu M, Gu X, Ma Z. Mitochondrial quality control in cerebral ischemia-reperfusion injury. *Mol Neurobiol.* 2021;58:5253-5271.
6. Pittas K, Vrachatis DA, Angelidis C, Tsoucala S, Giannopoulos G, Deftereos S. The role of calcium handling mechanisms in reperfusion injury. *Curr Pharm Des.* 2018;24:4077-4089.
7. Liu JC, Syder NC, Ghorashi NS, et al. EMRE is essential for mitochondrial calcium uniporter activity in a mouse model. *JCI Insight.* 2020;5:e134063.
8. Guan L, Che Z, Meng X, et al. MCU up-regulation contributes to myocardial ischemia-reperfusion injury through calpain/OPA-1-mediated mitochondrial fusion/mitophagy inhibition. *J Cell Mol Med.* 2019;23:7830-7843.
9. Bashaw GJ, Klein R. Signaling from axon guidance receptors. *Cold Spring Harb Perspect Biol.* 2010;2:a001941.
10. Dun XP, Parkinson DB. Role of Netrin-1 signaling in nerve regeneration. *Int J Mol Sci.* 2017;18:491.

11. Grenz A, Dalton JH, Bauerle JD, et al. Partial netrin-1 deficiency aggravates acute kidney injury. *PLoS One*. 2011;6:e14812.

12. Rosenberger P, Schwab JM, Mirakaj V, et al. Hypoxia-inducible factor-dependent induction of netrin-1 dampens inflammation caused by hypoxia. *Nat Immunol*. 2009;10:195-202.

13. Mao X, Xing H, Mao A, et al. Netrin-1 attenuates cardiac ischemia reperfusion injury and generates alternatively activated macrophages. *Inflammation*. 2014;37:573-580.

14. Zhang J, Cai H. Netrin-1 prevents ischemia/reperfusion-induced myocardial infarction via a DCC/ERK1/2/eNOS s1177/NO/DCC feed-forward mechanism. *J Mol Cell Cardiol*. 2010;48:1060-1070.

15. Yang X, Li S, Li B, et al. Netrin-1 overexpression improves neurobehavioral outcomes and reduces infarct size via inhibition of the notch1 pathway following experimental stroke. *J Neurosci Res*. 2017;95:1850-1857.

16. Chen J, Du H, Zhang Y, et al. Netrin-1 prevents rat primary cortical neurons from apoptosis via the DCC/ERK pathway. *Front Cell Neurosci*. 2017;11:387.

17. Zhao EY, Efendizade A, Cai L, Ding Y. The role of Akt (protein kinase B) and protein kinase C in ischemia-reperfusion injury. *Neurol Res*. 2016;38:301-308.

18. Li Y, Xiang L, Wang C, Song Y, Miao J, Miao M. Protection against acute cerebral ischemia/reperfusion injury by Leonuri Herba Total Alkali via modulation of BDNF-TrKB-PI3K/Akt signaling pathway in rats. *Biomed Pharmacother*. 2021;133:111021.

19. Yu ZH, Cai M, Xiang J, et al. PI3K/Akt pathway contributes to neuroprotective effect of Tongxinluo against focal cerebral ischemia and reperfusion injury in rats. *J Ethnopharmacol*. 2016;181:8-19.

20. Zheng Y, Wu Y, Liu Y, et al. Intrinsic effects of gold nanoparticles on oxygen-glucose deprivation/reperfusion injury in rat cortical neurons. *Neurochem Res*. 2019;44:1549-1566.

21. He X, Liu Y, Lin X, et al. Netrin-1 attenuates brain injury after middle cerebral artery occlusion via downregulation of astrocyte activation in mice. *J Neuroinflammation*. 2018;15:268.

22. Jin X, Luan H, Chai H, et al. Netrin1 interference potentiates epithelialtomesenchymal transition through the PI3K/AKT pathway under the hypoxic microenvironment conditions of nonsmall cell lung cancer. *Int J Oncol*. 2019;54:1457-1465.

23. Pareek G, Pallanck LJ. Inactivation of the mitochondrial protease Afg3l2 results in severely diminished respiratory chain activity and widespread defects in mitochondrial gene expression. *PLoS Genet*. 2020;16:e1009118.

24. Konig T, Troder SE, Bakka K, et al. The m-AAA protease associated with neurodegeneration limits MCU activity in mitochondria. *Mol Cell*. 2016;64:148-162.

25. Yan T, Zhao Y. Acetaldehyde induces phosphorylation of dynamin-related protein 1 and mitochondrial dysfunction via elevating intracellular ROS and Ca(2+) levels. *Redox Biol*. 2020;28:101381.

26. Maxwell JT, Tsai CH, Mohiuddin TA, Kwong JQ. Analyses of mitochondrial calcium influx in isolated mitochondria and cultured cells. *J Vis Exp*. 2018;134:57225.

27. Longa EZ, Weinstein PR, Carlson S, Cummins R. Reversible middle cerebral artery occlusion without craniectomy in rats. *Stroke*. 1989;20:84-91.

28. Yu J, Li X, Matei N, et al. Ezetimibe, a NPC1L1 inhibitor, attenuates neuronal apoptosis through AMPK dependent autophagy activation after MCAO in rats. *Exp Neurol*. 2018;307:12-23.

29. Zhao M, Hou S, Feng L, et al. Vinpocetine protects against cerebral ischemia-reperfusion injury by targeting astrocytic Connexin43 via the PI3K/AKT signaling pathway. *Front Neurosci*. 2020;14:223.

30. Kaur MM, Sharma DS. Mitochondrial repair as potential pharmacological target in cerebral ischemia. *Mitochondrion*. 2022;63:23-31.

31. Zhou X, Chen H, Wang L, et al. Mitochondrial dynamics: a potential therapeutic target for ischemic stroke. *Front Aging Neurosci*. 2021;13:721428.

32. Bano D, Ankarcrona M. Beyond the critical point: an overview of excitotoxicity, calcium overload and the downstream consequences. *Neurosci Lett*. 2018;663:79-85.

33. Cid-Castro C, Hernandez-Espinosa DR, Moran J. ROS as regulators of mitochondrial dynamics in neurons. *Cell Mol Neurobiol*. 2018;38:995-1007.

34. Zhao Q, Wang S, Li Y, et al. The role of the mitochondrial calcium uniporter in cerebral ischemia/reperfusion injury in rats involves regulation of mitochondrial energy metabolism. *Mol Med Rep*. 2013;7:1073-1080.

35. Movafagh S, Crook S, Vo K. Regulation of hypoxia-inducible factor-1a by reactive oxygen species: new developments in an old debate. *J Cell Biochem*. 2015;116:696-703.

36. Kma L, Baruah TJ. The interplay of ROS and the PI3K/Akt pathway in autophagy regulation. *Biotechnol Appl Biochem*. 2022;69:248-264.

37. Alzahrani AS. PI3K/Akt/mTOR inhibitors in cancer: At the bench and bedside. *Semin Cancer Biol*. 2019;59:125-132.

38. O'Donnell JS, Massi D, Teng MWL, Mandala M. PI3K-AKT-mTOR inhibition in cancer immunotherapy, redux. *Semin Cancer Biol*. 2018;48:91-103.